Multi-color Photometry, Roche Lobe Analysis and Period Study of the Overcontact Binary System, GW Bootis

Kevin B. Alton
UnderOak Observatory, 70 Summit Ave, Cedar Knolls, NJ 07927; kbalton@optonline.net

Received September 11, 2018; revised October 23, 2018; accepted October 25, 2018

Abstract GW Boo is a relatively bright (V-mag ~ 10.2) eclipsing W UMa binary system (P = 0.513544 d) which has surprisingly escaped detailed study since the first monochromatic light curve (LC) was published in 2003. LC data collected in 2011 and 2017 (B, V and I_c) at UnderOak Observatory (UO), produced eight new times-of-minimum for GW Boo which were used along with other eclipse timings from the literature to update the linear ephemeris. Secular variations (P_3 ~ 10.5y) in the orbital period suggested the possibility of a gravitationally bound third body. Roche modeling to produce synthetic LC fits to the observed data was accomplished using PHOEBE 0.31a and WDWINT 56a. In order to achieve the best synthetic fits to the multi-color LCs collected in 2011 and 2017 cool spot(s) were added to the Roche model.

1. Introduction

The variable behavior of GW Boo (GSC 1473-1049; BD+20°2890) was initially observed from data collected during the Semi-Automatic Variability Search (SAVS) (Maciejewski *et al*. 2003). Sparsely sampled photometric data for this system are available from the ROTSE-I survey (Akerlof *et al.* 2000; Wozniak *et al.* 2004; Gettel *et al.* 2006) as well as the ASAS survey (Pojmański *et al.* 2005). Although other times-of-minimum light have been sporadically published since 2008, this paper marks the first detailed period analysis and multi-color Roche model assessment of LCs for this system in the literature.

2. Observations and data reduction

Photometric collection dates at UnderOak Observatory (UO) included eight sessions between 03 June 2011 and 07 July 2011 with an additional 11-day imaging campaign conducted from 08 June 2017 to 26 June 2017. Instruments included a 0.2-m catadioptic telescope coupled with an SBIG ST-402ME CCD camera (2011) and a 0.28-m Schmidt-Cassegrain telescope (2017) equipped with an SBIG ST8-XME CCD camera; both were mounted at the Cassegrain focus. Automated imaging was performed with photometric B, V, and I_c filters sourced from SBIG and manufactured to match the Bessell prescription; the exposure time for all dark- and light-frames was 60 seconds in 2011 and 75 seconds in 2017. As is standard practice at UO, the computer clock was automatically synchronized to a reference clock immediately prior to each session. Image acquisition (lights, darks, and flats) was performed using CCDSOFT v5 (Software Bisque 2011) or THESKYX Pro Version 10.5.0 (Software Bisque 2018) while calibration and registration were performed with AIP4WIN v2.4.0 (Berry and Burnell 2005). Images of GW Boo were plate solved using the standard star fields (MPOSC3) provided in MPO CANOPUS v10.7.1.3 (Minor Planet Observer 2015) in order to obtain the magnitude (B, V, and I_c assignments for each comparison star. Only images taken above 30° altitude (airmass < 2.0) were accepted in order to minimize the effects of differential refraction and color extinction.

3. Results and discussion

3.1. Photometry and ephemerides

Five stars in the same field-of-view with GW Boo were used to derive catalog-based (MPOSC3) magnitudes in MPO CANOPUS (Table 1) using ensemble aperture photometry. During each imaging session comparison stars typically stayed within ± 0.011 mag for V and I_c filters and ± 0.016 mag for B passband.

A total of 397 photometric values in B, 421 in V, and 426 in I_c were acquired between 03 June 2011 and 07 July 2011 (Figure 1). The most recent campaign (08 June 2017–28 June 2017) produced 409 values in B, 395 in V, and 414 in I_c (Figure 2). Times-of-minimum were calculated using the method of Kwee and van Woerden (1956) as implemented in PERANSO v2.5 (Paunzen and Vanmunster 2016). Included in these determinations were eight new times-of-minimum for each filter which were averaged (Table 2) from each session. The Fourier routine (FALC; Harris *et al.* 1989) in MPO CANOPUS produced similar LC period solutions (0.531544 ± 0.000001 d) from both epochs. As appropriate, sparsely sampled photometric data from the ROTSE-I (clear filter) and ASAS (V-mag) surveys were converted from MJD to HJD and then normalized relative to V-mag data collected at UO in 2017. Period determinations from survey data were individually made from these data using PERANSO v2.5. The selected analysis method employed periodic orthogonal polynomials (Schwarzenberg-Czerny 1996) to fit observations and analysis of variance (ANOVA) to evaluate fit quality. The resulting orbital periods (P = 0.531544 ± 0.000008 d) were nearly identical and the folded curves remarkably superimposable (Figure 3). This provided an ideal opportunity to interpolate additional times-of-minimum from the survey data. A total of four values, two from each survey, that were closest to a mid-point bisecting line during Min I and Min II were weighted (50%) relative to directly observed new minima acquired at UO and published values (Table 2). These were used to analyze eclipse timings from 1999 through 2017 in which the reference epoch (Kreiner 2004) employed for calculating eclipse timing differences (ETD) was defined by the following linear ephemeris (Equation 1):

$$\text{Min.I(HJD)} = 2452500.335 + 0.5315444\ E. \quad (1)$$

Table 1. Astrometric coordinates (J2000) and color indices (B-V) for GW Boo and five comparison stars used in this photometric study.

Star Identification	*R.A. (J2000)* *h m s*	*Dec. (J2000)* *° ‘ “*	*V-mag*[a]	*(B–V)*[a]
GW Boo	13 53 13.85	+20 09 43.19	10.20	0.443
TYC 1473-1027-1	13 53 08.59	+20 07 24.00	11.38	0.478
GSC 1473-1036	13 53 19.14	+20 12 43.49	11.92	0.482
GSC 1473-0037	13 53 46.71	+20 11 17.99	12.85	0.258
TYC 1473-0024-1	13 53 43.79	+20 10 02.26	11.64	0.442
GSC 1473-0018	13 53 51.60	+20 08 18.60	12.29	0.569

Note: a. V-mag and (B–V) for comparison stars derived from MPOSC3 which is a hybrid catalog that includes a large subset of the Carlsberg Meridian Catalog *(CMC-14) as well as from the* Sloan Digital Sky Survey *(SDSS). Stars with BVI$_c$ magnitudes derived from* 2MASS *J–K magnitudes have an internal consistency of ± 0.05 mag. for V, ± 0.08 mag. for B, ± 0.03 mag. for I$_c$, and ± 0.05 mag. for B–V (Warner 2007).*

Table 2. Calculated differences (ETD)$_1$ following linear least squares fit of observed times-of-minimum for GW Boo and cycle number between 07 June 1999 and 28 June 2017.

HJD = 2400000+	*Cycle No.*	*ETD$_1$*[a]	*Reference*
51336.7680	–2189	–0.01631	NSVS (Wozniak *et al.* 2004)[b]
51620.8784	–1654.5	–0.01639	NSVS (Wozniak *et al.* 2004)[b]
52750.6864	471	–0.00601	ASAS (Pojmański *et al.* 2005)[b]
52751.7460	473	–0.00950	Otero 2004
52755.4724	480	–0.00388	SAVS (Maciejewski *et al.* 2003)[c]
52767.4280	502.5	–0.00804	SAVS (Maciejewski *et al.* 2003)[c]
52788.4237	542	–0.00835	Maciejewski *et al.* 2003
53462.6857	1810.5	–0.01044	ASAS (Pojmański *et al.* 2005)[b]
54555.8090	3867	–0.00819	Diethelm 2010
55294.3962	5256.5	–0.00194	Hübscher and Monninger 2011
55310.4066	5286.5	0.06213	Hübscher and Monninger[d] 2011
55310.5829	5287	–0.02734	Hübscher and Monninger[d] 2011
55352.8640	5366.5	–0.00402	Diethelm 2010
55631.9288	5891.5	–0.00003	Diethelm 2011
55687.4748	5996	–0.00045	Hoňková K. *et al.* 2013
55698.3703	6016.5	–0.00158	Nagai 2012
55702.3597	6024	0.00123	Nagai 2012
55711.3947	6041	–0.00002	Nagai 2012
55715.6468	6049	–0.00032	This study
55719.6324	6056.5	–0.00124	This study
55720.6960	6058.5	–0.00079	This study
55749.6671	6113	0.00115	This study
56001.8846	6587.5	0.00087	Diethelm 2012
56056.3663	6690	–0.00078	Hoňková K. *et al.* 2013
56074.7055	6724.5	0.00018	Diethelm 2012
56418.3519	7371	0.00313	Hübscher 2013
56764.3830	8022	–0.00118	Hübscher and Lehmann 2015
57119.4516	8690	–0.00424	Hübscher 2017
57128.4893	8707	–0.00279	Hübscher 2017
57489.4087	9386	–0.00204	Hübscher 2017
57516.5166	9437	–0.00290	Hübscher 2017
57859.0953	10081.5	–0.00457	Nagai 2018
57914.6423	10186	–0.00392	This study
57919.6904	10195.5	–0.00552	This study
57931.6506	10218	–0.00508	This study
57932.7142	10220	–0.00456	This study

Notes: a. (ETD)$_1$ = Eclipse Time Difference between observed time-of-minimum and that calculated using the reference ephemeris (Equation 1). b. Interpolated from superimposition of NSVS, ASAS, and UO2017 lightcurves (see Figure 3). c. Times-of-minimum determined from BD+20°2890 lightcurves in SAVS database. d. Outliers not included in analysis.

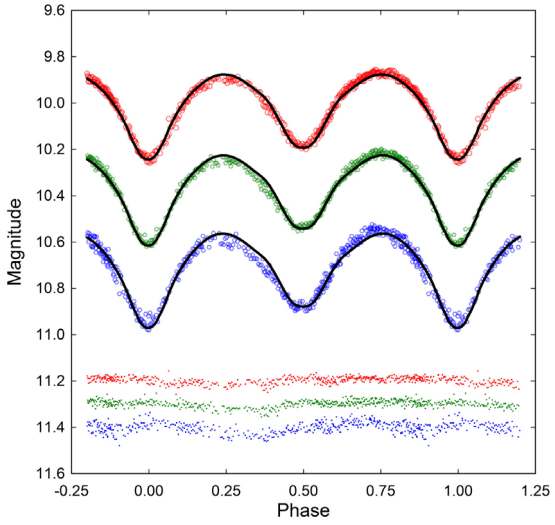

Figure 1. Folded CCD light curves for GW Boo produced from photometric data obtained between 03 June 2011 and 07 July 2011. The top (I$_c$), middle (V), and bottom curve (B) shown above were reduced to MPOSC3-based catalog magnitudes using MPO CANOPUS (Minor Planet Observer 2015). In this case, the Roche model assumed an A-type overcontact binary with no spots; residuals from the model fits are offset at the bottom of the plot to keep the values on scale.

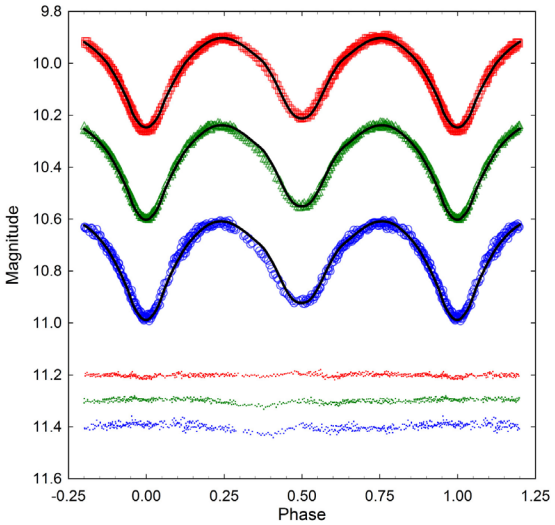

Figure 2. Folded CCD light curves for GW Boo produced from photometric data obtained between 06 June 2017 and 28 June 2017. The top (I$_c$), middle (V), and bottom curve (B) shown above were reduced to MPOSC3-based catalog magnitudes using MPO CANOPUS. In this case, the Roche model assumed an A-type overcontact binary with no spots; residuals from the model fits are offset at the bottom of the plot to keep the values on scale.

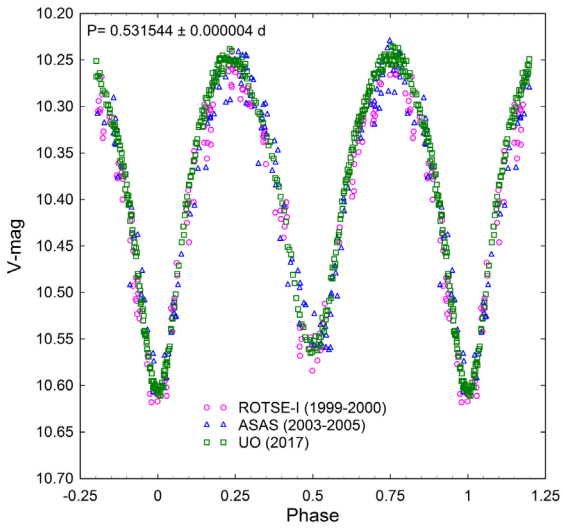

Figure 3. Folded (P = 0.531544 d) CCD light curves for GW Boo produced from sparsely sampled photometric data acquired during the ROTSE-I (1999–2000) and ASAS (2003–2005) surveys along with data generated at UO between 06 June 2017 and 28 June 2017.

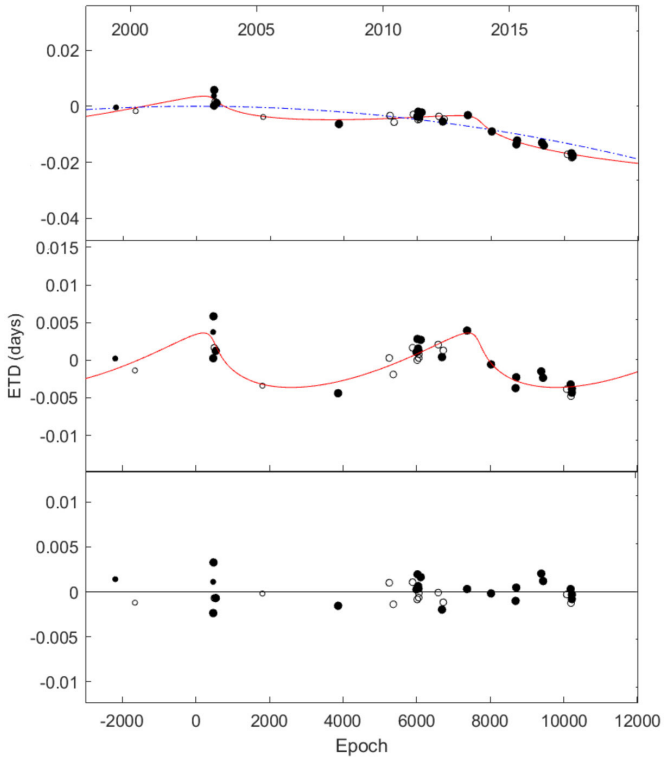

Figure 4. Eclipse timing differences (ETD) calculated using the reference ephemeris (Equation 2) cited by Kreiner (2004). LiTE analysis (top panel—solid line) for a putative third body where an elliptical path (e = 0.764) is predicted with an orbital period of 10.48 ± 0.01 y. The downwardly directed quadratic fit to the data is shown with a dashed line. Solid circles are from primary minima whereas open circles represent secondary minima. The center panel shows the LiTE fit after subtraction of the quadratic component. Residuals remaining from the model fit are plotted in the bottom panel.

An updated linear ephemeris (Equation 2) based on near-term (2013–2017) eclipse timing data was determined as follows:

$$\text{Min. I (HJD)} = 2457932.7138\ (39) + 0.5315423\ (4)E. \quad (2)$$

Secular variations in orbital period can sometimes be uncovered by plotting the difference between the observed eclipse times and those predicted by the reference epoch against cycle number (Figure 4). In this case the ETD residuals suggest there may be an underlying variability in the orbital period. This effect could potentially originate from magnetic cycles (Applegate 1992), the gravitational influence of a third body also known as the light-time effect (LiTE), or periodic mass transfer between either star. LiTE analysis was performed using the MATLAB (MathWorks©) code reported by Zasche *et al.* (2009) in which the associated parameters in the LiTE equation (Irwin 1959) were derived by simplex optimization. These include P_3 (orbital period of star 3 and the 1–2 pair about their common center of mass), orbital eccentricity *e,* argument of periastron ω, time of periastron passage T_0, and amplitude $A = a_{12} \sin i_3$ (where a_{12} = semimajor axis of the 1–2 pair's orbit about the center of mass of the three-star system, and i_3 = orbital inclination of the third body in a three-star system). For the sake of simplicity, a minimum mass for the putative third body was initially calculated after assuming a circular orbit (e = 0) which is co-planar ($i_3 = 90°$) with the binary pair. These results (LiTE-1) summarized in Table 3 suggest the presence of a stellar object with a mass approximating 0.21 $M_\odot$. According to tabulations by Harmanec (1988) and similar information on stellar mass by Pecaut and Mamajeck (2013) this third body is most likely an M-class star. A stellar object this small would only provide a slight excess in luminance ($L_3 < 0.07\%$); therefore no third light (l_3) contribution would be expected during Roche modeling of the light curves (section 3.4). The results (Table 3; Figure 4) with the lowest residual sum of squares (LiTE-2) predict a third body orbiting elliptically (e = 0.764 ± 0.197) every 10.48 ± 0.01 y. Similar to the case where e = 0, the fractional luminosity contributed by a gravitationally bound third body with minimum mass of 0.28 $M_\odot$ would still not reach significance during Roche modeling.

Alternatively, the sinusoidal variations in the orbital period of the binary pair may be due to magnetic activity cycles attributed to Applegate (1992). However, according to an empirical relationship (Equation 3) between the length of orbital period modulation and angular velocity ($\omega = 2\pi / P_{orb}$):

$$\log P_{mod}[y] = 0.018 - 0.36 \log (2\pi / P_{orb}\ [s] \quad (3)$$

(Lanza and Rodonò 1999) any period modulation resulting from a change in the gravitational quadrupole moment would probably be closer to 25 years for GW Boo, not the much shorter period ($P_3 < 10.5$ y) estimated from LiTE analyses.

Another revelation from the LiTE analysis is that the sign of the quadratic coefficient (c_2) is negative thereby indicating that the period is slowly decreasing with time. Based upon the results for LiTE-2 (Table 3), this translates into a orbital period decrease (dP/dt) approaching 1.8×10^{-7} d/y or 0.01556 s/y.

It is worth noting that eclipse timing data for GW Boo are only available for the past 18 years. This is not long enough

to complete two cycles assuming that the proposed sinusoidal variability ($P_3 \sim 10$ y) is correct. As a result, careful examination of the data summarized in Table 3 reveals significant error in the LiTE-1 parameter estimates which became notably better for an elliptical orbit (LiTE-2). Another decade of eclipse timings will probably be needed to solidify a LiTE solution for this system.

3.2. Effective temperature estimation

Interstellar extinction (A_V) was estimated according to the model described by Amôres and Lépine (2005). In this case the value for A_V (0.085) corresponds to a target positioned at Galactic coordinates l = 9.9936° and b = +74.2456° which is located within 400 pc as determined from parallax (Gaia DR2: Brown *et al.* 2018). Color index (B–V) data collected at UO and those acquired from an ensemble of nine other sources (Table 4) were corrected using the estimated reddening value (A_V / 3.1 = E(B–V) = 0.027 ± 0.001). The median intrinsic value ($(B–V)_0$ = 0.323 ± 0.012) which was adopted for Roche modeling indicates a primary star with an effective temperature (7080 K) that ranges in spectral type between F0V and F1V. This result is in good agreement with the Gaia DR2 release of stellar parameters (Andrae *et al.* 2018) in which the nominal T_{eff} for GW Boo is reported to be 6977 K. In contrast, an earlier study (Maciejewski *et al.* 2003) defines this system as a hotter (T_{eff} = 7650 K) and much larger spectral class A9III star based on an optical spectrum. According to the new results described herein, this classification is believed to be in error. It should be noted that luminosity classification of mid- to late A-type stars is especially difficult when trying to distinguish between dwarfs and giants (Gray and Corbally 2009). Furthermore, the mass of an A9 giant would approach 5 $M_\odot$ with a solar luminosity in excess of 26 $L_\odot$. As will be shown in the next section, the A9III assignment is rejected based on the mass, size, and luminosity obtained in this study and supported by other data included ($R_\odot$ and $L_\odot$) in the Gaia DR2 release of stellar parameters (Andrae *et al.* 2018).

Table 3. Putative third-body solution to the light-time effect (LiTE) observed as sinusoidal-like changes in GW Boo eclipse timings.

Parameter	*Units*	*LiTE-1*	*LiTE-2*
HJD_0	—	2452500.3236 (9)	24552500.3242 (9)
P_3	[y]	9.84 (35)	10.48 (1)
A (semi-amplitude)	[d]	0.0034 (14)	0.0036 (4)
ω	°	—	146 (17)
e_3	—	0	0.764 (197)
a_{12} sin i	[AU]	0.597 (250)	0.812 (86)
$f(M_3)$(mass function)	$M_\odot$	0.0022 (22)	0.0049 (1)
M_3 (i = 90°)	$M_\odot$	0.211 (161)	0.282 (1)
M_3 (i = 60°)	$M_\odot$	0.247 (72)	0.330 (2)
M_3 (i = 30°)	$M_\odot$	0.455 (144)	0.621 (3)
c_2 (quadratic coeff.)	$\sim 10^{-10}$	–0.877 (1)	–1.31 (1)
dP/dt	10^{-7} d/yr	–1.205 (1)	–1.8 (1)
Sum of squared residuals	—	0.000531	0.000491

3.3. Roche modeling approach

Roche modeling of LC data from GW Boo was primarily accomplished using the programs PHOEBE 0.31a (Prša and Zwitter 2005) and WDWINT 56a (Nelson 2009), both of which feature a user-friendly interface to the Wilson-Devinney WD2003 code (Wilson and Devinney 1971; Wilson 1990). WDWINT 56a makes use of Kurucz's atmosphere models (Kurucz 1993) which are integrated over $UBVR_cI_c$ optical passbands. In both cases, the selected model was Mode 3 for an overcontact binary. Bolometric albedo ($A_{1,2}$ = 0.5) and gravity darkening coefficients ($g_{1,2}$ = 0.32) for cooler stars (7500 K) with convective envelopes were respectively assigned according to Ruciński (1969) and Lucy (1967). Since T_{eff1} for the primary (7080 K) approaches the transition temperature where stars are in radiative equilibrium, modeling with $A_{1,2}$ and $g_{1,2}$ fixed at 1 was also explored. Logarithmic limb darkening coefficients (x_1, x_2, y_1, y_2) were interpolated (Van Hamme 1993) following any change in the effective temperature (T_{eff2}) of the secondary star during model fit optimization. All but the temperature of the more massive star (T_{eff1}), $A_{1,2}$ and $g_{1,2}$ were allowed to vary during DC iterations. In general, the best fits for T_{eff2}, i, q and Roche potentials ($\Omega_1 = \Omega_2$) were collectively refined (method of multiple subsets) by DC using the multicolor LC data. In general LCs from 2011 (Figures 1 and 5) and 2017 (Figures 2 and 6) exhibit significant asymmetry that is most obvious in the B-passband. This suggests the presence of spots (Yakut and Eggleton 2005) which were added during Roche modeling to address distorted/asymmetric regions in the LCs.

3.4 Roche modeling results

GW Boo would appear to be an A-type overcontact system in which the primary star (m_1) is not only the more massive but also the hottest. The deepest minimum (Min I) occurs when the primary star is eclipsed by its smaller binary partner. These results are consistent with the general observation (Csizmadia and Klagyivik 2004; Skelton and Smits 2009) that A-type overcontact binaries have a mass ratio $m_2 / m_1 < 0.3$, are hotter than the Sun with spectral types ranging from A to F, and orbit the center-of-mass with periods varying between 0.4 to 0.8 d. Although a total eclipse is very nearly observed (Figures 7 and 8) there is some risk at attempting to determine a photometric mass ratio (q_{ptm}) by Roche modeling with the WD code alone (Terrell and Wilson 2005). They point out that even when the eclipses are "very slightly partial, the accuracy of a q_{ptm}

Table 4. Estimation of effective temperature (Teff1) of GW Boo based upon dereddened (B-V) data from six surveys, two published reports and the present study.

	USNO-B1.0	*All Sky Combined*	*2MASS*	*APASS*	*Terrell* et al. *2005*	*Tycho*	*UCAC4*	*Oja (1985)*	*Present Study*
$(B–V)_0$	0.323	0.391	0.273	0.321	0.311	0.399	0.322	0.333	0.348
T_{eff1}[a] (K)	7077	6715	7328	6622	7130	6685	7083	7036	6955
Spectral Class[a]	F0V-F1V	F3V-F4V	F0V-F1V	F4V-F5V	F0V-F1V	F3V-F4V	F0V-F1V	F0V-F1V	F1V-F2V

Note: a. T_{eff1} interpolated and spectral class range estimated from Pecaut and Mamajek (2013). Median value, $(B–V)_0$ = 0.323 ± 0.012, corresponds to an F0V-F1V primary star (T_{eff1} = 7080 ± 263 K).

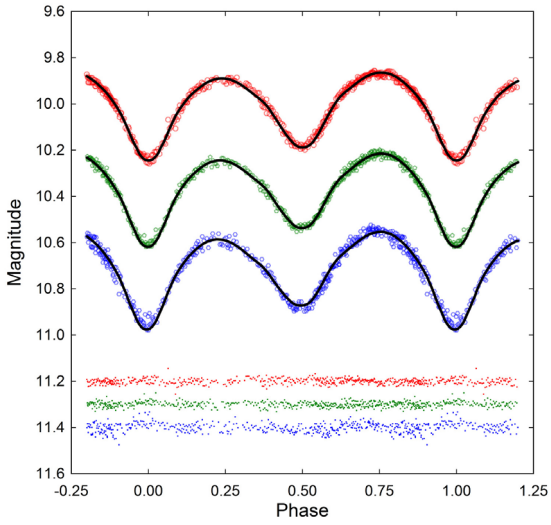

Figure 5. Folded CCD light curves for GW Boo produced from photometric data obtained between 03 June 2011 and 07 July2011. The top (I_c), middle (V), and bottom curve (B) shown above were reduced to MPOSC3-based catalog magnitudes using MPO CANOPUS. In this case, the Roche model assumed an A-type overcontact binary with a cool spot on the secondary star; residuals from the model fits are offset at the bottom of the plot to keep the values on scale.

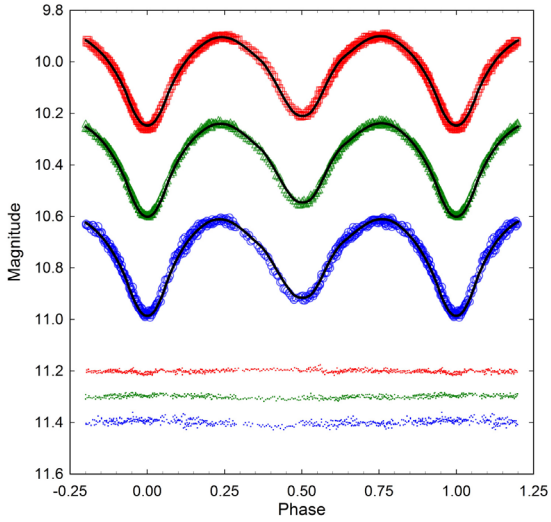

Figure 6. Folded CCD light curves for GW Boo produced from photometric data obtained between 08 June 2017 and 26 June 2017. The top (I_c), middle (V), and bottom curve (B) shown above were reduced to MPOSC3-based catalog magnitudes using MPO CANOPUS. In this case, the Roche model assumed an A-type overcontact binary with a single cool spot each on the primary and secondary stars; residuals from the model fits are offset at the bottom of the plot to keep the values on scale.

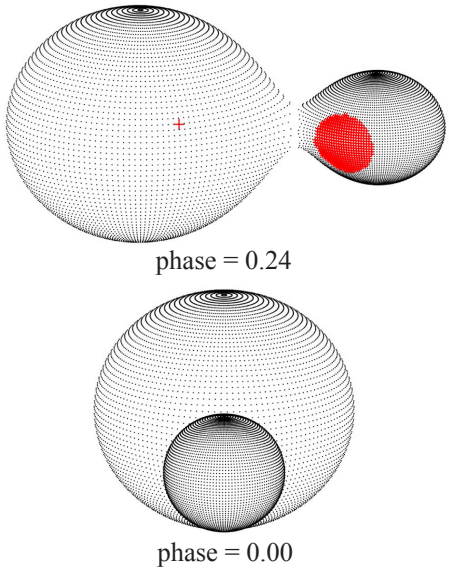

Figure 7. Spatial model of GW Boo from the 2011 LC (V-mag) illustrating the transit at Min I ($\varphi = 0$) and cool spot location ($\varphi = 0.24$) on the secondary star.

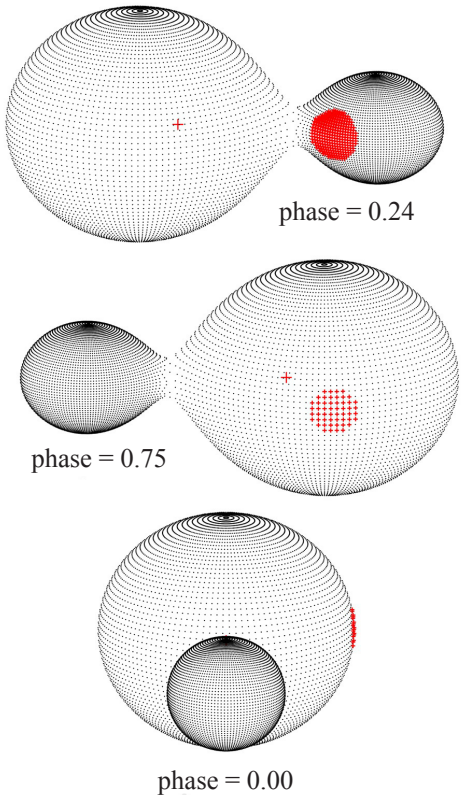

Figure 8. Spatial model of GW Boo from the 2017 LC (V-mag) showing the transit at Min I ($\varphi = 0$) and cool spot locations on the primary ($\varphi = 0.75$) and secondary stars ($\varphi = 0.24$).

drops dramatically." Given this proviso, modeling data collected with different equipment six years apart resulted in a mean best fit for the mass ratio (m_2/m_1) where $q = 0.196 \pm 0.007$. Despite this good agreement, without the luxury of radial velocity data it is not possible to unequivocally determine the mass ratio for GW Boo or accurately establish the total mass.

Modeling under the assumption that GW Boo possesses a radiative envelope ($A_{1,2}$ and $g_{1,2} = 1$) did not yield an improved fit compared to a system in convective equilibrium where $A_{1,2}$ and $g_{1,2}$ are respectively assigned values of 0.5 and 0.32. Only the latter LC parameters and geometric elements determined for each of these model fits (2011 and 2017) are summarized in Table 5. It should be noted that the listed errors only reflect the model fit to the observations which assumed exact values for all fixed parameters. The results are improbably low considering the estimated uncertainty (± 263 K) associated with the adopted T_{eff1} (Table 4) along with basic assumptions about $A_{1,2}$ and $g_{1,2}$ and the influence of putative spots added to the Roche model.

The fill-out parameter (f) which corresponds to a volume percent of the outer surface shared between each star was calculated according to Equation 4 (Kallrath and Milone 1999; Bradstreet 2005) where:

$$f = (\Omega_{inner} - \Omega_{1,2}) / (\Omega_{inner} - \Omega_{outer}). \quad (4)$$

Ω_{outer} is the outer critical Roche equipotential, Ω_{inner} is the value for the inner critical Roche equipotential and $\Omega = \Omega_{1,2}$ denotes the common envelope surface potential for the binary system. In this case the constituent stars are considered overcontact since $0 < f < 1$. Spatial models rendered with BINARY BAKER3 (Bradstreet and Steelman 2004; using the physical and geometric elements from the best fit spotted Roche models are shown in Figure 7 (2011) and Figure 8 (2017).

3.5. Absolute parameters

Preliminary absolute parameters (Table 6) were derived for each star in this system using results from the best fit simulations (spotted model) of the 2011 and 2017 LCs. In the absence of RV data, total mass can not be unequivocally calculated; however, stellar mass and radii estimates from main sequence stars have been published over a wide range of spectral types. This includes a value ($M_1 = 1.56 \pm 0.07\ M_\odot$) interpolated from Harmanec (1988) and another ($M_1 = 1.55 \pm 0.04\ M_\odot$) from Pecaut and Mamajek (2013). Additionally, three different empirical period-mass relationships for W UMa-binaries have been published by Qian (2003) and later by Gazeas and Stępień (2008) and Gazeas (2009). According to Qian (2003) the mass of the primary star (M_1) can be determined from Equation 5:

$$\log M_1 = 0.761(150) \log P + 1.82\,(28), \quad (5)$$

where P is the orbital period in days and leads to $M_1 = 1.73 \pm 0.21\ M_\odot$ for the primary. The mass-period relationship (Equation 6) derived by Gazeas and Stępień (2008):

$$\log M_1 = 0.755\,(59) \log P + 0.416\,(24). \quad (6)$$

corresponds to a W UMa system where $M_1 = 1.62 \pm 0.11\ M_\odot$. Gazeas (2009) reported another empirical relationship (Equation 7) for the more massive (M_1) star of a contact binary such that:

$$\log M_1 = 0.725\,(59) \log P - 0.076\,(32) \log q + 0.365\,(32). \quad (7)$$

In this case the mass for the primary star was estimated to be $1.66 \pm 0.16\ M_\odot$. A final relationship reported by Torres *et al.* (2010) for main sequence stars above 0.6 $M_\odot$ predicts a mass of 1.55 $M_\odot$ for the primary constituent. The median of these six values ($M_1 = 1.59 \pm 0.04\ M_\odot$) was used for subsequent determinations of M_2, semi-major axis a, volume-radius r_L, bolometric magnitude M_{bol}, and ultimately distance d (pc) to GW Boo. The secondary mass = $0.31 \pm 0.01\ M_\odot$ and total mass ($1.90 \pm 0.04\ M_\odot$) of the system were subsequently determined using the mean photometric mass ratio (0.196 ± 0.007). By comparison, a stand-alone main sequence star with a mass similar to the secondary (early M-type) would likely be much smaller ($R_\odot \sim 0.4$), cooler ($T_{eff} \sim 3600$), and far less luminous ($L_\odot \sim 0.03$). The mean semi-major axis, $a(R_\odot) = 3.42 \pm 0.03$, was calculated from Newton's version (Equation 8) of Kepler's third law where:

$$a^3 = (G \times P^2\,(M_1 + M_2)) / (4\pi^2). \quad (8)$$

The effective radii of each Roche lobe (r_1) can be calculated to over the entire range of mass ratios ($0 < q < \infty$) according to an expression (Equation 9) derived by Eggleton (1983):

$$r_L = (0.49q^{2/3}) / (0.6q^{2/3} + ln\,(1 + q^{1/3})). \quad (9)$$

from which values for r_1 (0.5212 ± 0.0001) and r_2 (0.2514 ± 0.0001) were determined for the primary and secondary stars, respectively. Since the semi-major axis and the volume radii are known, the solar radii for both binary constituents can be calculated where $R_1 = a \cdot r_1 = (1.79 \pm 0.01\ R_\odot)$ and $R_2 = a \cdot r_2 = (0.85 \pm 0.01\ R_\odot)$.

Luminosity in solar units ($L_\odot$) for the primary (L_1) and secondary stars (L_2) were calculated from the well-known relationship (Equation 10) where:

$$L_{1,2} = (R_{1,2} / R_\odot)^2\,(T_{1,2} / T_\odot)^4. \quad (10)$$

Assuming that $T_{eff1} = 7080$ K, mean $T_{eff2} = 6689$ K and $T_\odot = 5772$ K, then the solar luminosities for the primary and secondary are $L_1 = 7.27 \pm 0.11$ and $L_2 = 1.37 \pm 0.02$, respectively. According to the Gaia DR2 release of stellar parameters (Andrae *et al.* 2018), T_{eff} (6977 K) is slightly cooler than the adopted T_{eff1} (7080 K) while the size ($R_\odot = 1.92$) and luminosity ($L_\odot = 7.90$) of the primary star in GW Boo are slightly greater than the values estimated by this study. By any measure these results are far removed from those expected from the A9III classification proposed by Maciejewski *et al.* (2003).

3.6. Distance estimates to GW Boo

The bolometric magnitudes ($M_{bol1,2}$) for the primary and secondary were determined according to Equation 11 such that:

$$M_{bol1,2} = 4.75 - 5 \log(R_{1,2} / R_\odot) - 10 \log(T_{1,2} / T_\odot). \quad (11)$$

Table 5. Synthetic light curve parameters evaluated by Roche modeling and the geometric elements derived for GW Boo, an A-type W UMa variable.

Parameter	*2011 No spot*	*2011 Spotted*	*2017 No spot*	*2017 Spotted*
T_{eff1} (K)[b]	7080	7080	7080	7080
T_{eff2} (K)	6662 ± 8	6606 ± 6	6766 ± 4	6771 ± 3
q (m_2 / m_1)	0.196 ± 0.001	0.206 ± 0.001	0.190 ± 0.001	0.192 ± 0.001
A[b]	0.5	0.5	0.5	0.5
g[b]	0.32	0.32	0.32	0.32
$\Omega_1 = \Omega_2$	2.190 ± 0.002	2.210 ± 0.002	2.188 ± 0.001	2.184 ± 0.001
i°	75.03 ± 0.19	75.03 ± 0.14	73.83 ± 0.09	74.67 ± 0.09
$A_S = T_S / T_\star$[c]	—	—	—	0.86 ± 0.01
Θ_S (spot co—latitude)[c]	—	—	—	90 ± 1.5
φ_S (spot longitude)[c]	—	—	—	95 ± 2
r_S (angular radius)[c]	—	—	—	11 ± 0.1
$A_S = T_S / T_\star$[d]	—	0.75 ± 0.01	—	0.80 ± 0.01
Θ_S (spot co—latitude)[d]	—	95.5 ± 2.1	—	86.8 ± 1.6
φ_S (spot longitude)[d]	—	59.4± 2.2	—	49.1 ± 2.3
r_S (angular radius)[d]	—	30 ± 0.6	—	25 ± 0.4
$L_1 / (L_1 + L_2)_B$[e]	0.8534 ± 0.0003	0.8529 ± 0.0003	0.8472 ± 0.0001	0.8444 ± 0.0001
$L_1 / (L_1 + L_2)_V$	0.8445 ± 0.0001	0.8425 ± 0.0001	0.8407 ± 0.0001	0.8378 ± 0.0001
$L_1 / (L_1 + L_2)_{Ic}$	0.8334 ± 0.0001	0.8297 ± 0.0001	0.8328 ± 0.0001	0.8296 ± 0.0001
r_1 (pole)	0.4964 ± 0.0001	0.4937 ± 0.0001	0.4956 ± 0.0001	0.4971 ± 0.0001
r_1 (side)	0.5431 ± 0.0002	0.5396 ± 0.0002	0.5417 ± 0.0001	0.5439 ± 0.0001
r_1 (back)	0.5678 ± 0.0003	0.5651 ± 0.0002	0.5653 ± 0.0001	0.5684 ± 0.0001
r_2 (pole)	0.2399 ± 0.0008	0.2447 ± 0.0005	0.2347 ± 0.0003	0.2383 ± 0.0003
r_2 (side)	0.2507 ± 0.0009	0.2559 ± 0.0007	0.2448 ± 0.0004	0.2489 ± 0.0003
r_2 (back)	0.2915 ± 0.0020	0.2980 ± 0.0015	0.2820 ± 0.0008	0.2891 ± 0.0007
Fill—out factor (%)	25.6	28.4	16.2	24.2
RMS (B)[f]	0.02414	0.02012	0.01295	0.01102
RMS (V)[f]	0.01586	0.01175	0.00853	0.00700
RMS (I_c)[f]	0.01500	0.01200	0.00647	0.00630

Notes: a. All error estimates for T_{eff2}, q, $\Omega_{1,2}$, A_S, Θ_S, φ_S, r_S, $r_{1,2}$, and L_1 from WDWINT 56a (Nelson 2009).
b. Fixed during DC.
c. Primary spot temperature, location and size parameters in degrees.
d. Secondary spot temperature, location and size parameters in degrees.
e. L_1 and L_2 refer to scaled luminosities of the primary and secondary stars, respectively.
f. Monochromatic root mean square deviation of model fit from observed values (mag).

Table 6. Preliminary absolute parameters (±SD) for GW Boo using the mean photometric mass ratio ($q_{ptm} = m_2 / m_1$) from the Roche model fits of LC data (2011 and 2017) and estimated mass for an F0V-F1V primary star.

Parameter	*Primary*	*Secondary*
Mass ($M_\odot$)	1.59 ± 0.04	0.31 ± 0.01
Radius ($R_\odot$)	1.79 ± 0.01	0.85 ± 0.01
a ($R_\odot$)	3.42 ± 0.03	—
Luminosity ($L_\odot$)	7.27 ± 0.11	1.37 ± 0.02
M_{bol}	2.60 ± 0.02	4.41 ± 0.02
Log (g)	4.13 ± 0.01	4.06 ± 0.01

This led to values where $M_{bol1} = 2.61 \pm 0.01$ and $M_{bol2} = 4.42 \pm 0.01$. Combining the bolometric magnitudes resulted in an absolute magnitude ($M_V = 2.43 \pm 0.01$) after adjusting with the bolometric correction (BC = –0.010) interpolated from Pecaut and Mamajek (2013). Substituting into the distance modulus (Equation 12):

$$d(pc) = 10^{((m - Mv - Av + 5) / 5)}, \quad (12)$$

where $m = V_{max}$ (10.23 ± 0.01) and $A_V = 0.085$ leads to an estimated distance of 349 ± 2 pc to GW Boo. This value is about 12% lower than the distance (398 ± 9 pc) calculated directly from the second release (DR2) of parallax data from the Gaia mission (Lindegren *et al.* 2016; Brown *et al.* 2018). Considering that LC magnitudes were not determined using absolute photometry and perhaps more importantly the physical size/luminosity were not derived from a spectroscopic (RV) mass ratio, this discrepancy is not unreasonable.

4. Conclusions

Eight new times-of-minimum were observed based on CCD data collected with B, V, and I_c filters. These along with other published values led to an updated linear ephemeris for GW Boo. Potential changes in orbital periodicity were assessed using eclipse timings which only cover a 18-year time span. Nevertheless, an underlying sinusoidal variability ($P_3 \sim 10.5$ y) in the orbital period was uncovered which suggests the possibility of a third gravitationally bound but much smaller stellar object. The intrinsic color, $(B–V)_0$, determined from this study and eight other sources indicates that the effective temperature for the primary is ~7080 K which corresponds to a spectral class ranging from F0V to F1V. This A-type overcontact system very nearly experiences a total eclipse. Therefore the photometric mass ratio determined by Roche modeling (q = 0.196 ± 0.007) may suffer in accuracy based on precautions noted by Terrell and Wilson (2005). Radial velocity findings will be required

to unequivocally determine a spectroscopically derived mass ratio and total mass for the system. GW Boo is bright enough (V_{mag} ~10.2) to be considered a viable candidate for further spectroscopic study to unequivocally classify this system and generate RV data to refine (or refute) the absolute parameter values presented herein.

5. Acknowledgements

This research has made use of the SIMBAD database operated at Centre de Données astronomiques de Strasbourg, France. Time-of-minima data tabulated in the Variable Star Section of the Czech Astronomical Society (B.R.N.O.) website proved invaluable to the assessment of potential period changes experienced by this variable star. In addition, the Northern Sky Variability Survey hosted by the Los Alamos National Laboratory, the International Variable Star Index maintained by the AAVSO, the Semi-Automatic Variability Search at the Nicolaus Copernicus University, and the ASAS Catalogue of Variable Stars were mined for photometric data. The diligence and dedication shown by all associated with these organizations is very much appreciated. This work also presents results from the European Space Agency (ESA) space mission Gaia. Gaia data are being processed by the Gaia Data Processing and Analysis Consortium (DPAC). Funding for the DPAC is provided by national institutions, in particular the institutions participating in the Gaia MultiLateral Agreement (MLA). The Gaia mission website is https://www.cosmos.esa.int/gaia. The Gaia archive website is https://archives.esac.esa.int/gaia. Furthermore, the author greatly appreciates the review, corrections and suggested changes made by an anonymous referee.

References

Akerlof, C., *et al.* 2000, *Astron. J.*, **119**, 1901.
Amôres, E. B., and Lépine, J. R. D. 2005, *Astron. J.*, **130**, 650.
Andrae, R., *et al.* 2018, *Astron. Astrophys.*, **616A**, 8.
Applegate, J. H. 1992, *Astrophys. J.*, **385**, 621.
Berry, R., and Burnell, J. 2005, *The Handbook of Astronomical Image Processing*, 2nd ed., Willmann-Bell, Richmond, VA.
Bradstreet, D. H. 2005, in *The Society for Astronomical Sciences 24th Annual Symposium on Telescope Science*, Society for Astronomical Sciences, Rancho Cucamonga, CA, 23.
Bradstreet, D. H., and Steelman, D. P. 2004, BINARY MAKER 3, Contact Software (http://www.binarymaker.com).
Brown, A. G. A., *et al.* 2018, *Astron. Astrophys.*, **616A**, 1.
Csizmadia, Sz., and Klagyivik, P. 2004, *Astron. Astrophys.*, **426**, 1001.
Diethelm, R. 2010, *Inf. Bull. Var. Stars*, No. 5945, 1.
Diethelm, R. 2011, *Inf. Bull. Var. Stars*, No. 5992, 1.
Diethelm, R. 2012, *Inf. Bull. Var. Stars*, No. 6029, 1.
Eggleton, P. P. 1983, *Astrophys. J.*, **268**, 368.
Gazeas, K. D. 2009, *Commun. Asteroseismology*, **159**, 129.
Gazeas, K., and Stępień, K. 2008, *Mon. Not. Roy. Astron. Soc.*, **390**, 1577.
Gettel, S. J., Geske, M. T., and McKay, T. A. 2006, *Astron. J.*, **131**, 621.
Gray, R. O., and Corbally, C. J. 2009, *Stellar Spectral Classification*, Princeton Univ. Press, Princeton, NJ.
Harmanec, P. 1988, *Bull. Astron. Inst. Czechoslovakia*, **39**, 329.
Harris, A. W., *et al.* 1989, *Icarus*, **77**, 171.
Hoňková K., *et al.* 2013, *Open Eur. J. Var. Stars*, **160**, 1.
Hübscher, J. 2013, *Inf. Bull. Var. Stars*, No. 6084, 1.
Hübscher, J. 2017, *Inf. Bull. Var. Stars*, No. 6196, 1.
Hübscher, J., and Lehmann, P. B. 2015, *Inf. Bull. Var. Stars*, No. 6149, 1.
Hübscher, J., and Monninger, G. 2011, *Inf. Bull. Var. Stars*, No. 5959, 1.
Irwin, J. B. 1959, *Astron. J.*, **64**, 149.
Kallrath, J., and Milone, E. F. 1999, *Eclipsing Binary Stars: Modeling and Analysis*, Springer, New York.
Kreiner, J. M. 2004, *Acta Astron.*, **54**, 207.
Kurucz, R. L. 1993, *Light Curve Modeling of Eclipsing Binary Stars*, ed. E. F. Milone, Springer-Verlag, New York, 93.
Kwee, K. K., and van Woerden, H. 1956, *Bull. Astron. Inst. Netherlands*, 12, 327.
Lanza, A. F., and Rodonò, M. 1999, *Astron. Astrophys.*, **349**, 887.
Lindegren, L., *et al.* 2016, *Astron. Astrophys.*, **595A**, 4.
Lucy, L. B. 1967, *Z. Astrophys.*, **65**, 89.
Maciejewski, G., Czart, K., Niedzielski, A., and Karska, A. 2003, *Inf. Bull. Var. Stars*, No. 5431, 1.
Nagai. K. 2012, *Bull. Var. Star Obs. League Japan*, No. 53, 1.
Nagai. K. 2018, *Bull. Var. Star Obs. League Japan*, No. 64, 1.
Nelson, R. H. 2009, WDWINT version 56a astronomy software (https://www.variablestarssouth.org/bob-nelson).
Otero, S. A. 2004, *Inf. Bull. Var. Stars*, No. 5532, 1.
Paunzen, E., and Vanmunster, T. 2016, *Astron. Nachr.*, **337**, 239.
Pecaut, M. J., and Mamajek, E. E. 2013, *Astrophys. J. Suppl. Ser.*, **208**, 9.
Pojmański, G., Pilecki, B., and Szczygiel, D. 2005, *Acta Astron.*, **55**, 275.
Prša, A., and Zwitter, T. 2005, *Astrophys. J.*, **628**, 426.
Qian, S.-B. 2003, *Mon. Not. Roy. Astron. Soc.*, **342**, 1260.
Ruciński, S. M. 1969, *Acta Astron.*, **19**, 245.
Schwarzenberg-Czerny, A. 1996, *Astrophys. J., Lett.*, **460**, L107.
Skelton, P. L., and Smits, D. P. 2009, *S. Afr. J. Sci.*, **105**, 120.
Terrell, D., and Wilson, R. E. 2005, *Astrophys. Space Sci.*, **296**, 221.
Torres, G., Andersen, J., and Giménez, A. 2010, *Astron. Astrophys. Rev.*, 18, 67.
Van Hamme, W. 1993, *Astrophys. J.*, **106**, 2096.
Warner, B. 2007, *Minor Planet Bull.*, **34**, 113.
Wilson, R. E. 1990, *Astrophys. J.*, **356**, 613.
Wilson, R. E., and Devinney, E. J. 1971, *Astron. J.*, **143**, 1.
Wozniak, P. R., *et al.* 2004, *Astron. J.*, **127**, 2436.
Yakut, K., and Eggleton, P. P. 2005, *Astrophys. J.*, **629**, 1055.
Zasche, P., Liakos, A., Niarchos, P., Wolf, M., Manimanis, V., and Gazeas, K. 2009, *New Astron.*, **14**, 121.